Published by Avanti Publishers

Journal of Advanced Thermal Science Research

ISSN (online): 2409-5826

Fabrication and Investigation of Novel Cu_2O-doped $CaCO_3$ Composites-based Thermochemical Energy Storage System for Concentrating Solar Power Application

Azhar Abbas Khosa[1], Xinyue Han[1,*] and Ghulam Abbas Ashraf[2]

[1]*School of Energy and Power Engineering, Jiangsu University, Zhenjiang, Jiangsu 212013, China*
[2]*New Uzbekistan University, Mustaqillik Ave. 54, Tashkent 100007, Uzbekistan*

ARTICLE INFO

Article Type: Research Article

Academic Editor: Mehdi Kabir

Keywords:
Catalysis
Kinetic Analysis
Thermal energy storage
Non-isothermal methods
Physical characterizations

Timeline:
Received: October 30, 2024
Accepted: December 05, 2024
Published: December 17, 2024

Citation: Khosa AA, Han X, Ashraf GA. Fabrication and investigation of novel Cu_2O-doped $CaCO_3$ composites-based thermochemical energy storage system for concentrating solar power application. J Adv Therm Sci Res. 2024; 11: 53-64.

DOI: https://doi.org/10.15377/2409-5826.2024.11.3

ABSTRACT

The limited solar energy absorption capacity of $CaCO_3$ hinders its efficacy in thermochemical energy storage (TCES) systems for concentrated solar power (CSP) facilities. This study aims to tackle this problem by introducing Cu_2O as a dopant in $CaCO_3$. Cu_2O possesses a bandgap that is more conducive to solar absorption. This study examines the structural, optical, and thermal characteristics of $CaCO_3$ doped with Cu_2O to improve its effectiveness in TCES applications. Therefore, the current study investigates the sunlight absorption of $CaCO_3$ material after doping Cu_2O. Cu_2O in $CaCO_3$ is doped and its UV, FTIR, and XRD characteristics are analyzed. Furthermore, non-isothermal and isothermal calcination was conducted to determine the kinetics and lower the calcination temperature limit. The results reveal that Cu_2O introduced no new phase in $CaCO_3$, and XRD data confirmed it. UV data reveals that the Cu_2O-doped $CaCO_3$ has a bandgap of 5.01 eV, while pure $CaCO_3$ has a bandgap of 5.30 eV. According to the kinetic analysis, Cu_2O-doped $CaCO_3$ follows the three-dimensional diffusion (D3) model. Its activation energy is 644.3 kJ/mol, while pure $CaCO_3$ follows the D1 model, and its activation energy is calculated as 234.8 kJ/mol. The lowest calcination temperature limit for pure and Cu_2O-doped $CaCO_3$ samples is 750°C. Hence, the proposed material is recommended for use in thermal energy storage applications.

*Corresponding Author
Email: hanxinyue123456@163.com
Tel: +(86) 13812458751

1. Introduction

Concentrated solar power (CSP) plants are being installed to fulfil the energy demands because they are potentially worthy of generating dispatchable renewable electricity [1, 2]. Solar tower systems are predicted to contribute 11% to the global electricity demand by 2050, which amounts to 954–1080 GW [3]. CSP plants operate smoothly after integrating a thermal energy storage (TES) system and the use of TES systems in operational CSP plants is found to be 40%. In the case of under-construction and newly planned CSP plants, the demand for TES systems has risen to 80% [4]. These power plants use a molten salt-based TES system, which absorbs concentrated solar energy and is stored in an insulated tank for later use. Molten salt-based TES systems are simple, but they limit the plant's performance because of the maximum temperature limit of 560°C (above this temperature, salt degrades). Hence, the efficiency of the electricity generation cycle becomes limited. Furthermore, salt corrodes plant material and its solidification temperature is around 220°C; hence, it requires extra energy to regulate the temperature above this threshold [5-8]. Therefore, a better TES system with fewer limitations is needed. Some interesting TES systems and their applications are discussed in these studies [9].

A thermochemical energy storage (TCES) system is a potential candidate because it is noncorrosive, has high energy storage density and can operate at temperatures above 600°C [10, 11]. These advantages make it superior to sensible TES systems [12-14] and latent TES systems [15, 16]. In the TCES system, energy is charged when the material's endothermic decomposition occurs and the energy is discharged due to a reversible exothermic synthesis reaction. The commonly used TCES reaction pairs are metal redox [17, 18], carbonates [19, 20], hydrides [21], sulphur [22], ammonia [23], methanol [24] and hydroxides [25]. The $CaCO_3$/CaO reaction pair, a carbonate-based TCES material, is chosen for investigation because it is abundant and cheap [26, 27], has high energy storage density and reaction enthalpy and its working temperature is higher than 900°C [19]. When integrated with a CSP, its operation starts by concentrating the sunlight on $CaCO_3$, which absorbs the thermal energy at the required high temperature and decomposes endothermically into CaO and CO_2. These products are stored until the stored energy is required to meet electricity demand [28]. CO_2 and CaO are allowed to react exothermically upon energy demand and the thermal energy is discharged, which further produces electricity. Therefore, the $CaCO_3$/CaO TCES system, also known as the calcium looping (CaL) process, is suitable for commercial applications [26, 27, 29]. Its chemical equation is given below:

$$CaCO_3 \leftrightharpoons CaO + CO_2\ ;\ \Delta H_{r,298K} = \pm 177.8\ kJ/mol \tag{1}$$

The performance of the $CaCO_3$/CaO TCES system is dependent on factors like reaction environment [30], reaction temperature [31], particle size [32] and reaction duration [33]. These parameters directly affect the material's reactivity and improving any of them can improve the system's efficiency. This can be achieved by pretreatment of reactants [5] and using dopants in $CaCO_3$ [34]. These techniques aim to avoid the sintering of particles, which affects the reversible carbonation of CaO by restricting the diffusion of CO_2. The sintering of particles occurs when the calcination of $CaCO_3$ occurs at temperatures above 800°C. Therefore, doping inert materials in $CaCO_3$ has been found to be helpful in improving the calcination reaction rate. Various inert materials, for example, Li_2SO_4 [35], SiO_2 [36], $Ca_3Al_2O_6$ [37], AlOOH [38], TiO_2 [39], ZnO [34], MgO [40] and CeO_2 [41], have been investigated for their effects on the calcination reaction of $CaCO_3$ and its kinetics. The following paragraph discusses the effects of these dopants on the kinetics of the calcination of $CaCO_3$.

Jin *et al*. [38] doped AlOOH in $CaCO_3$ and investigated its effects on the kinetics of the calcination reaction. The composite material followed the one-dimensional diffusion (D1) model and the new activation energy was 301.4 kJ/mol. Similarly, Chen *et al*. [42] and Shui *et al*. [43] doped SiO_2 in $CaCO_3$, and their findings about the kinetics reveal that the reaction follows the D1 model. The value of activation energy determined by Chen *et al*. [42] is 212.9 kJ/mol and by Shui *et al*. [43] is 155 kJ/mol. Elsewhere, Yanase *et al*. [41] investigated the effects of CeO_2 on the reaction kinetics of the $CaCO_3$ and found that the calcination reaction occurs under the three-dimensional diffusion (D3) model while the activation energy is 40 kJ/mol. Mathew *et al*. [44] tested the $CaCO_3/Al_2O_3$ composite in a reactor and reported its activation energy as 215.21 kJ/mol at 0.6 bar. The reaction kinetics of the composite followed the Avrami model with exponent 3. All these studies investigated the kinetic analysis using Coats-Redfern (CRF) integral method and Achar-Brindly-Sharp (ABS) differential method equations [45, 46]. Some researchers

investigated the kinetics of the $CaCO_3$ using the Kissinger method [47]. Khosa *et al*. added SiO_2 [48] and ZnO [34] in $CaCO_3$ separately and studied the effects of both dopants using the Kissinger method, which yielded activation energies of 123.6 and 149.7 kJ/mol, respectively. Similarly, Xu *et al*. [49] studied the effects of TiO_2 on the kinetics of $CaCO_3$ and reported its activation energy to be 149.75 kJ/mol. All these studies used a dopant material to investigate its effects on the kinetics of the $CaCO_3$ and its parameters.

Therefore, Cu_2O was chosen as a dopant for $CaCO_3$ and investigated its kinetics using CRF and ABS equations. To the best of our knowledge, Cu_2O has not been used in $CaCO_3$/CaO-based TCES systems. This material was selected because its melting point (~1508 K [50]) is higher than the calcination temperature of $CaCO_3$ (950°C [48]). Furthermore, it has a bandgap of 2 eV [51], which makes it capable of absorbing most of the solar spectrum. This property of Cu_2O can help improve the sunlight absorption capability of $CaCO_3$. Cu_2O is also an abundantly found non-toxic material.

This study investigates the effects of Cu_2O dopant on the $CaCO_3$/CaO TCES system. In this regard, the kinetic analysis of the pure and Cu_2O-doped $CaCO_3$ samples is performed and their calcination reaction rate equations are formulated. The effect of Cu_2O dopant on the UV absorption and crystal structure of $CaCO_3$ is also investigated. Furthermore, calcination at various temperatures helps determine the lowest calcination temperature at which $CaCO_3$ stores energy efficiently. FTIR analysis is conducted to observe the functional groups in the composite materials.

2. Material Preparation and Experimental Methods

To produce Cu_2O-doped $CaCO_3$ composite materials, specific quantities of Cu_2O and $CaCO_3$ were measured following the necessary ratios. Cu_2O amounts in weight percentages such as 0.5%, 1%, 2%, and 5% were doped in $CaCO_3$, and the samples were labelled as CCu1, CCu2, CCu3, and CCu4, respectively. Subsequently, the measured quantities were amalgamated in a mortar. The mixture was manually crushed for 30 minutes using a pestle to guarantee comprehensive blending and achieve a homogeneous dispersion of the nanoparticles. The mechanical grinding procedure enhances the close interaction between Cu_2O and $CaCO_3$ particles, facilitating the creation of composite nanoparticles. The Cu_2O-doped $CaCO_3$ composites were collected and analyzed to define their characteristics and assess their potential applications.

The composites were analyzed for their phase and structural properties using X-ray diffraction (XRD: D8-ADVANCE Da-Vinci), Fourier Transform Infrared Spectroscopy (FTIR: Nicolet 6700) and UV-Vis-NIR (LAMBDA 750) spectrophotometry. XRD with Cu-Kα radiation was used to identify the crystalline structure. FTIR, employing the KBr pellet method, was utilized to examine the chemical composition across a range of wavelengths from 400 to 3700 cm^{-1}. The UV-Vis-NIR spectrophotometer analyzed absorption spectra and energy bandgap within the 250 to 800 nm wavelength range. Thermogravimetric analysis (TGA: NETZSCH STA 449) is used to investigate the thermal characteristics of nanoparticles. This method quantifies the alteration in the mass of the nanoparticles concerning temperature. This analysis reveals the nanoparticles' thermal stability, composition and decomposition temperatures. The data acquired by TGA can be utilized to comprehend and enhance the thermal characteristics of the nanoparticles for diverse applications. For kinetic analysis of pure and Cu_2O-doped $CaCO_3$, non-isothermal calcination of samples was carried out from 20°C to 950°C at various heating rates i.e., 2.5, 5, 10,15, and 30 K/min. Similarly, isothermal calcination of pure and Cu_2O-doped $CaCO_3$ samples was performed at 650, 675, 700, 725, and 750°C to determine the lower limit of calcination temperature.

2.1. Kinetic Analysis of the Calcination Process

The following equation represents the reaction rate of solid-gas reaction pairs for non-isothermal conditions. The ICTAC committee [52] endorses this equation, which helps determine the reaction rate via Arrhenius parameters for any heating rate and temperature. The equation is given as below:

$$\frac{dX}{dT} = \left(\frac{A}{\beta}\right) exp\left(-\frac{E}{RT}\right) f(X) \tag{2}$$

where X, T, A, β, E, and R represent conversion, temperature, pre-exponential factor, heating rate, activation energy, and ideal gas constant, respectively. Similarly, $\frac{dX}{dT}$ is change in conversion with the change in temperature and $f(X)$ is a function dependent on conversion. X is determined from thermogravimetric data obtained from TGA using the following equation:

$$X = \left(1 - \frac{w_t}{w_0}\right) \times \frac{M_{CaCO_3}}{M_{CO_2}} \tag{3}$$

where w and M are the weight of the sample and molecular mass of the material, respectively. The subscripts t, 0, $CaCO_3$ and CO_2 depict the time of weight measurement, the time before starting the experiment (initial value), solid calcium carbonate material and carbon dioxide gas, respectively.

2.2. Model Recognition

CRF [45] and ABS [46] methods are based on integral ($g(X)$) and differential ($f(X)$) functions of the conversion (X), respectively. Both are used to determine the kinetics of the thermal decomposition (calcination) reaction of the pure and Cu_2O-doped $CaCO_3$. Non-isothermal TGA data is used for this purpose. The equations for CRF and ABS methods are given below:

CRF method

$$ln\left[\frac{g(X)}{T^2}\right] = ln\left(\frac{AR}{\beta E}\right) - \frac{E}{RT} \tag{4}$$

ABS method

$$ln\left[\frac{d(X)}{f(X)dT}\right] = ln\left(\frac{A}{\beta}\right) - \frac{E}{RT} \tag{5}$$

Kinetic parameters, such as activation energy E and pre-exponential factor A, are determined using CRF and ABS equations. In these equations, β and T are the experimental conditions and X is the result obtained from the TGA data. R is the ideal gas constant, and its value is constant. Therefore, only two parameters E and A are the unknowns, and there are two equations to determine them. In this regard, Vyazovkin *et al*. [52] provided a list of kinetic models along with their corresponding differential ($f(X)$) and integral ($g(X)$) forms, as given in Table **1**. CRF and ABS equations are solved using the listed models (Table **1**) and a suitable model is selected based on the regression coefficient (R^2). The logarithmic term in both equations is plotted against $\frac{1}{T}$ and the equations are solved like a regression equation ($y = a + bx$). According to the regression equation form, $ln\left(\frac{A}{\beta}\right)$ is the y-intercept and $-\frac{E}{R}$ is the slope of the plot. Therefore, E and A are calculated accordingly and used in the kinetic equation for the calcination reaction of pure and Cu_2O-doped $CaCO_3$. For kinetic analysis, the non-isothermal thermogravimetric data were obtained at various heating rates, i.e., 2.5, 5, 10, 15, and 30 °C/min.

Table 1: Decomposition kinetic models used to determine the calcination kinetics of pure and Cu_2O-doped $CaCO_3$.

Decomposition Model	*g(X)*	*f(X)*	Model Code
Mample (1st order)	$-\ln(1-X)$	$(1-X)$	F1
Contracting cylinder	$1-(1-X)^{1/2}$	$2(1-X)^{1/2}$	R2
Contracting sphere	$1-(1-X)^{1/3}$	$3(1-X)^{2/3}$	R3
Avarami-Erofeev	$[-\ln(1-X)]^{1/2}$	$2[-\ln(1-X)]^{1/2}(1-X)$	A2
Avarami-Erofeev	$[-\ln(1-X)]^{1/3}$	$3[-\ln(1-X)]^{2/3}(1-X)$	A3
One-dimensional diffusion	X^2	$\frac{1}{2}X^{-1}$	D1
Two-dimensional diffusion	$(1-X)\ln(1-X)+X$	$[-\ln(1-X)]^{-1}$	D2
Three-dimensional diffusion	$[1-(1-X)^{1/3}]^2$	$\frac{3}{2}\left[1-(1-X)^{1/3}\right]^{-1}(1-X)^{2/3}$	D3

3. Results and Discussion

3.1. Physical Characterizations (XRD, UV and FTIR)

XRD investigation offers detailed information about the crystalline structure and phase composition of the produced nanoparticles, as shown in Fig. (**1**). XRD pattern for Cu_2O has distinct peaks at 2θ values of 29.72°, 36.76°, 42.6°, 43.6°, 61.48°, and 73.62°. The observed peaks agree with the distinctive crystal planes of Cu_2O, which are consistent with the established diffraction data for Cu_2O as documented in Joint Committee on Powder Diffraction Standards (JCPDS) card number 05-0667. The detected peaks provide evidence of the existence of Cu_2O and its crystalline arrangement in the sample. XRD pattern of $CaCO_3$ has peaks at 2θ values of 23.22°, 29.6°, 36.16°, 39.6°, 43.34°, 47.66°, 48.68°, and 57.56°. The peaks observed in the data correspond to the conventional diffraction pattern of $CaCO_3$, as indicated by the JCPDS card with the reference number 05-0586. The observed pattern confirms the presence of $CaCO_3$ in the sample and verifies that it retains its anticipated crystalline form. The XRD pattern of the Cu_2O-doped $CaCO_3$ composite displays the distinctive peaks associated with both Cu_2O and $CaCO_3$, providing evidence of the successful formation of the composite material. These peaks indicate that the composite maintains the crystalline structures of its constituent components. Crucially, no extra peaks are detected in the composite, indicating that the synthesis method did not introduce any new stages or unforeseen chemical processes. The finding suggests that the composite is a thoroughly blended combination of Cu_2O and $CaCO_3$, with no notable alterations in its composition [53-55].

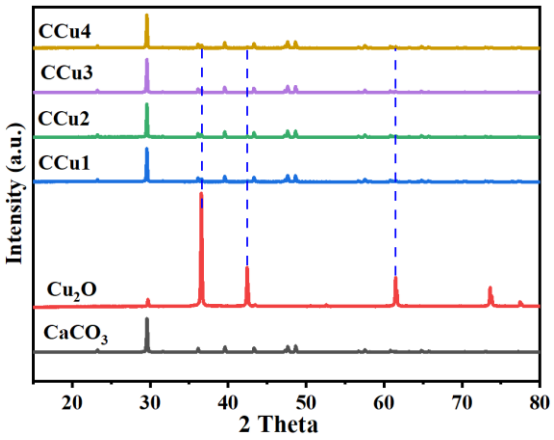

Figure 1: XRD data of pure and Cu_2O-doped $CaCO_3$ samples.

UV-Vis spectroscopy investigation yields significant insights into the produced materials' optical characteristics and band gaps, essential for comprehending their future uses. The UV-visible absorbance spectra (Fig. **2**) and Tauc's plots of $(\alpha h\upsilon)^2$ vs photon energy for the band gap energy of nanoparticles are shown in (Fig. **2**). The UV-Vis study of Cu_2O indicates a band gap of 1.95 eV. The tiny difference in energy levels between the valence band and the conduction band suggests that this material has the potential to be used as a semiconductor with excellent capabilities for absorbing visible light. The absorption spectra of Cu_2O exhibit substantial absorption in the visible region, in line with its band gap, enabling its utilization in diverse optoelectronic applications. The UV-Vis study of $CaCO_3$ reveals a band gap of 5.30 eV. The high band gap of this material indicates that it has a broad bandgap, which restricts its ability to absorb light to the UV range. The high band gap of $CaCO_3$ is characteristic of insulating materials and indicates its restricted use in processes driven by visible light. Copper(I) oxide encapsulated within a calcium carbonate composite: The Cu_2O and $CaCO_3$ composite (CCu4) material exhibits a bandgap of 5.01 eV. The bandgap of this material is lower than that of pure $CaCO_3$ but higher than that of Cu_2O. Compared to $CaCO_3$ alone, the decrease in bandgap can be ascribed to Cu_2O, which brings energy levels within the bandgap that enable absorption in the visible range. Nevertheless, the composite maintains a significant bandgap, suggesting that although certain optical features of Cu_2O affect the composite, the material as a whole still has characteristics more akin to an insulator rather than a semiconductor with a low bandgap. The bandgap study examines the distinct optical characteristics of Cu_2O, $CaCO_3$ and their composite, offering valuable insights into their prospective applications in fields including photocatalysis, sensing and optoelectronics [56-58].

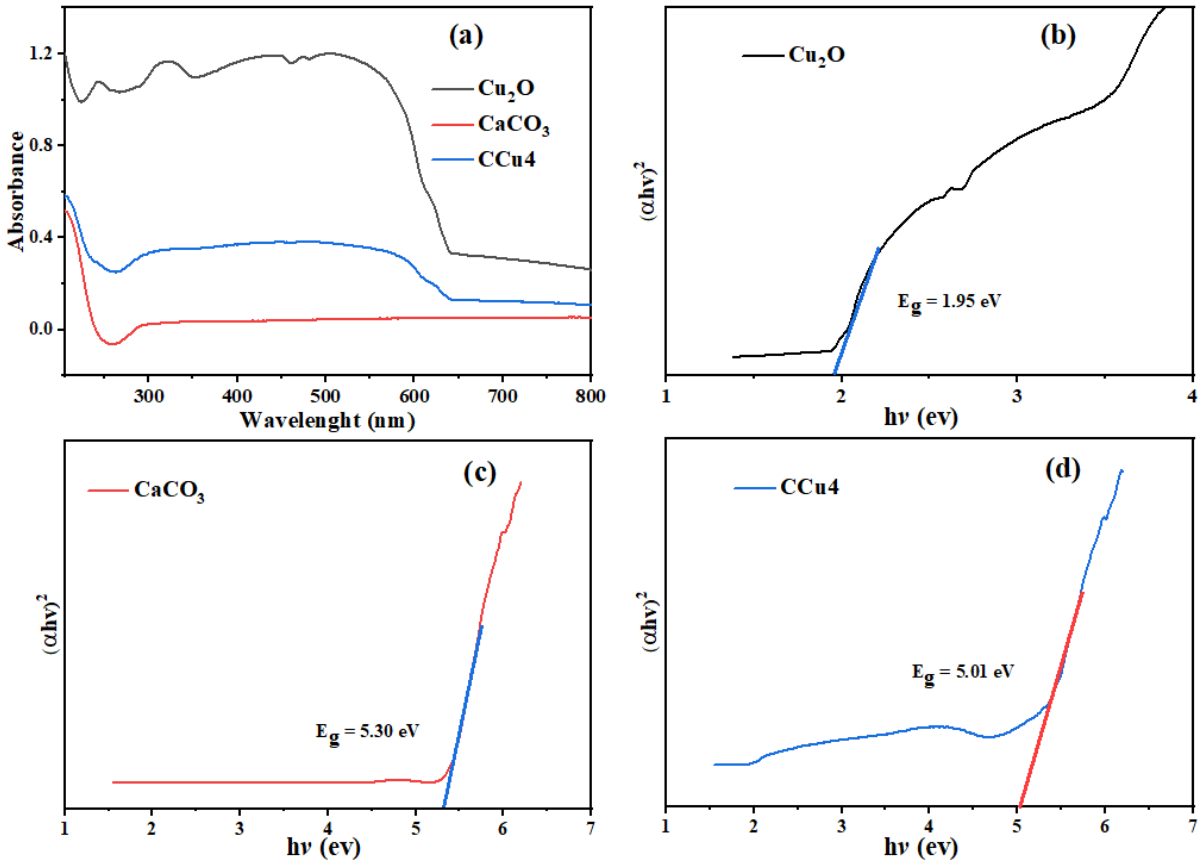

Figure 2: (**a**) UV-visible absorbance spectra, and (**b-d**) Tauc's plots of $(\alpha h\upsilon)^2$ versus photon energy for bandgap energy of samples.

FTIR analysis offers valuable information about the produced materials' functional groups and bonding properties. The FTIR spectrum of Cu_2O exhibits a distinct transmittance peak around 600 cm^{-1}, which signifies the specific Cu-O bond stretching vibrations that are associated with copper(I) oxide (Fig. **3**) [59]. The FTIR spectrum of the Cu_2O and $CaCO_3$ composite (CCu3-4) exhibits numerous notable peaks, including intense transmittance peaks at 649 cm^{-1}, 872 cm^{-1}, and 1391 cm^{-1}. The peak observed at 649 cm^{-1} is ascribed to the vibrations of the Ca-O bond, whilst the peaks at 872 cm^{-1} and 1391 cm^{-1} are associated with the vibrations of the carbonate group (CO_3^{2-}) in $CaCO_3$ (Fig. **3**) [60]. These data validate the existence of both Cu_2O and $CaCO_3$ in the composite and offer insights into the bonding environments of the individual materials.

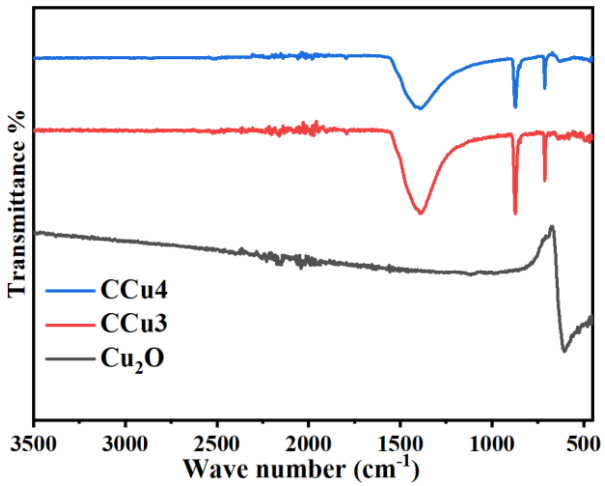

Figure 3: FTIR data of Cu_2O and its composites with $CaCO_3$.

3.2. Effect of Cu_2O Loadings on the Calcination of $CaCO_3$

The calcination of $CaCO_3$ was performed to study the impact of the Cu_2O dopant on it and its loading amount varied from 0.5% to 5%. All the samples were calcined non-isothermally from 20°C to 950°C at 10 K/min. The mass percentage of different samples doped with Cu_2O is shown in Fig. (**4**). The calcination reaction rate differs for various amounts of loading in the sample. In this case, the sample loaded with 1% Cu_2O depicts the highest reaction rate and hence is considered for kinetic analysis performed in the current study. The extent of the calcination reaction yielded by Cu_2O doped samples i.e., 0.5, 1, 2, and 5%, is 57.36, 59.26, 59.11, and 58.37, respectively. Cu_2O directly affects the heat transport phenomenon within the $CaCO_3$ because of which the calcination temperature by the material is achieved quickly and hence, the reaction rate improves.

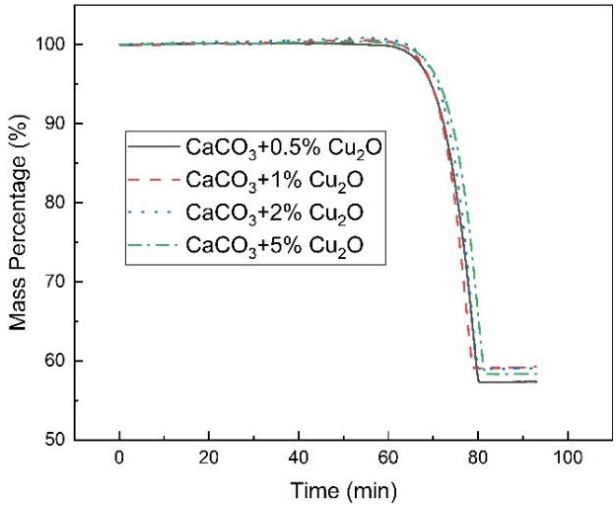

Figure 4: Effect of Cu_2O dopant applied on $CaCO_3$ in various loadings.

3.3. Suitable Model and Relevant Equations

Regression analysis was performed for all the models tabulated in Table **1**. Consequently, a model yielding the maximum R^2 value for the CRF and ABS equations is considered the most suitable model to represent the kinetic equation of the calcination reaction. The three models with R^2 values higher than 0.97 for the pure $CaCO_3$ are shortlisted and provided in Table **2**. The D1 model is considered the best-suited model because its R^2 values for CRF and ABS equations are the highest. Therefore, the values of E and A yielded by the D1 model are 234.8 kJ/mol and 2.15×10^{14} s^{-1}, respectively. Furthermore, all the kinetic parameters determined against each heating rate for CRF and ABS equations are provided in detail in Table **3**. The data for the kinetics of the pure $CaCO_3$ is taken from our previous publication [36]. The kinetic equation for the calcination of pure $CaCO_3$ is given as follows:

$$\frac{dX}{dt} = (2.15 \times 10^{14}) \times exp\left(-\frac{234798.7}{RT}\right) \times \frac{1}{2}X^{-1} \quad (6)$$

Similarly, the three best-suited models for the Cu_2O-doped $CaCO_3$ are scrutinized and are listed in Table **2**. D3 has the highest values of R^2 for CRF and ABS equations, i.e., 0.93 and 0.99, respectively. Therefore, its kinetic parameters (E and A) are calculated for the D3 model and their values are 644.3 kJ/mol and 1.94×10^{43} s^{-1}, respectively. Furthermore, all the kinetic parameters determined against each heating rate for CRF and ABS equations are provided in detail in Table **3**. The kinetic equation for the calcination of Cu_2O-doped $CaCO_3$ is given as follows:

$$\frac{dX}{dt} = (1.94 \times 10^{43}) \times exp\left(-\frac{644339.1}{RT}\right) \times \frac{3}{2}\left[1-(1-X)^{1/3}\right]^{-1}(1-X)^{2/3} \quad (7)$$

Table 2: Top three models shortlisted based on R^2 values for pure and Cu_2O-doped $CaCO_3$.

Sample	Mean of R^2 (ABS Method)	Mean of R^2 (CRF Method)	Model
$CaCO_3$	0.99	0.99	D1
	0.99	0.98	R3
	0.98	0.99	D2
Cu_2O-doped $CaCO_3$	0.99	0.93	D3
	0.95	0.95	F1
	0.97	0.93	R3

Table 3: Kinetic parameters for the D1 and D3 models for pure and Cu_2O-doped $CaCO_3$.

Sample	β	CRF Method			ABS Method			Model
		E	lnA	R^2	E	lnA	R^2	
$CaCO_3$	5	292.53	33.17	0.996	225.68	24.98	0.989	D1
	10	311.18	34.58	0.992	228.60	24.65	0.989	
	15	173.05	18.22	0.989	177.75	19.20	0.976	
	mean	258.92	28.66	0.992	210.68	22.94	0.985	
Cu_2O-doped $CaCO_3$	2.5	765.12	86.7	0.91	462.06	62.3	0.97	D3
	5	662.02	73.1	0.99	658.19	85.3	0.99	
	10	497.98	52.07	0.98	586.78	75.04	0.99	
	15	940.41	101.9	0.83	541.56	68.7	0.99	
	30	763.85	81.7	0.95	565.42	72.01	0.99	
	mean	725.87	79.1	0.93	562.80	72.7	0.99	

Their calcination reaction at various temperatures is carried out to understand the performance of pure and Cu_2O-doped $CaCO_3$. This also helps find the lowest temperature at which the calcination reaction rate is better and the system stores energy efficiently. Fig. (**5**) shows the calcination curves for calcination temperatures such as 650, 675, 700, 725, and 750°C. It is evident from the results that both the pure and Cu_2O-doped $CaCO_3$ samples decompose slowly from 650°C to 725°C. Therefore, the energy charging process is slow and less efficient at these temperatures. At 750°C, both the samples depict a relatively high reaction rate. Hence, the energy charging process is fast and efficient at this temperature. It can be stated that the system must be operated at or above 750°C to achieve better charging efficiency.

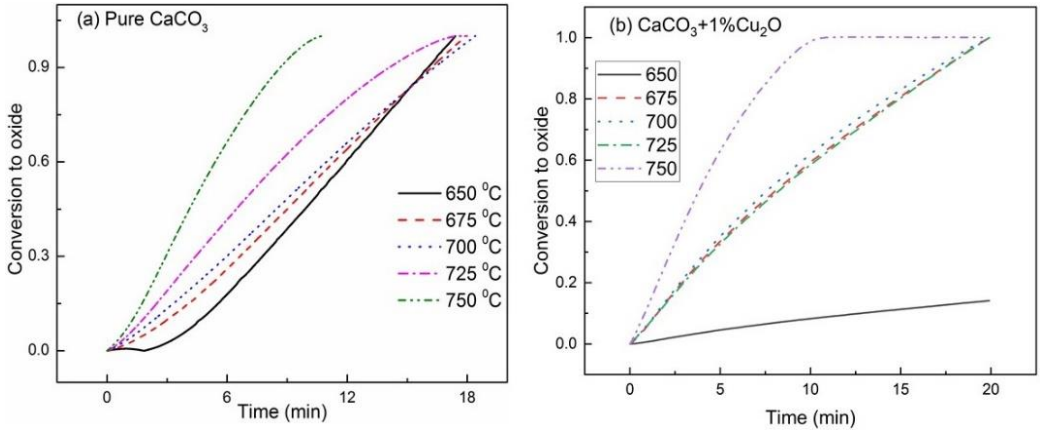

Figure 5: Performance analysis of pure and Cu_2O-doped $CaCO_3$ samples at various calcination temperatures.

4. Conclusion

The current study investigates the energy storage efficiency of pure and Cu_2O-doped $CaCO_3$ samples. Non-isothermal calcination of pure and Cu_2O-doped samples is performed to analyze the reaction kinetics. Isothermal calcination is carried out to determine the lower limit of calcination temperature at which $CaCO_3$ stores thermal energy efficiently. Furthermore, UV and XRD analyses characterize samples' light absorption and crystal structure, while FTIR analysis provides information about the functional groups of the material. The main conclusions are given below:

- XRD pattern of the Cu_2O-doped $CaCO_3$ composite displays the distinctive peaks associated with both Cu_2O and $CaCO_3$, providing evidence for the successful formation of the composite material. These peaks indicate that the composite maintains the crystalline structures of its constituent components. Crucially, no extra peaks are detected in the composite, indicating that the synthesis method did not introduce any new stages or unforeseen chemical processes.
- The UV-Vis study of $CaCO_3$ reveals a band gap of 5.30 eV. The high band gap of this material indicates that it has a broad bandgap, which restricts its ability to absorb light to the UV range. The high band gap of $CaCO_3$ is characteristic of insulating materials and indicates its restricted use in processes driven by visible light.
- The Cu_2O and $CaCO_3$ composite (CCu4) material exhibits a bandgap of 5.01 eV. The bandgap of this material is lower than that of pure $CaCO_3$ but higher than that of Cu_2O. Compared to $CaCO_3$ alone, the decrease in bandgap can be ascribed to the existence of Cu_2O, which brings energy levels within the bandgap that enable absorption in the visible range.
- The kinetic analysis reveals that pure $CaCO_3$ follows the D1 model, while Cu_2O-doped $CaCO_3$ decomposes according to the D3 model. The activation energy values of pure and Cu_2O-doped $CaCO_3$ are 234.8 and 644.3 kJ/mol.
- The lower limit of calcination temperature for both pure and Cu_2O-doped $CaCO_3$ is 750°C. At this temperature, both samples store thermal energy efficiently.

Conflict of Interest

No conflict of interest is associated with this manuscript.

Funding

This research work is funded by Jiangsu Excellent Postdoctoral Program (2022ZB638).

Acknowledgments

The authors acknowledge the support for Dr. Azhar Abbas Khosa’s living expenses and are thankful to the organization.

Data Availability

Data will be available on reasonable request.

Nomenclature and Abbreviations

ABS = Achar-Brindly-Sharp

AlOOH = Aluminium hydroxide oxide

CaL = Calcium looping

$CaCO_3$ = Calcium carbonate

CaO = Calcium oxide

CO_2 = Carbon dioxide

Cu_2O = Copper(I) oxide or cuprous oxide

$Ca_3Al_2O_6$ = Tricalcium aluminate

CeO_2 = Cerium(IV) oxide

CRF = Coats-Redfern

CSP = Concentrated solar power

D1 = One-dimensional diffusion model

D3 = Three-dimensional diffusion model

FTIR = Fourier Transform Infrared Spectroscopy

GW = Gigawatt

ICTAC = International Confederation for Thermal Analysis and Calorimetry

JCPDS = Joint Committee on Powder Diffraction Standards

Li_2SO_4 = Lithium sulfate

MgO = Magnesium oxide

SiO_2 = Silicon dioxide or silica

TCES = Thermochemical energy storage

TES = Thermal energy storage

TGA = Thermogravimetric analysis

TiO_2 = Titanium dioxide

UV = Ultraviolet

XRD = X-ray diffraction

ZnO = Zinc oxide

References

[1] International Energy Agency. Technology roadmap solar thermal electricity. OECD Publishing; 2015.

[2] International Renewable Energy Agency. Renewable power generation costs in 2020. eBook Partnership; 2022.

[3] del Río P, Peñasco C, Mir-Artigues P. An overview of drivers and barriers to concentrated solar power in the European Union. Renew Sustain Energy Rev. 2018; 81(1): 1019-29. https://doi.org/10.1016/j.rser.2017.06.038

[4] Ortiz C, Valverde JM, Chacartegui R, Perez-Maqueda LA. Carbonation of limestone derived CaO for thermochemical energy storage: from kinetics to process integration in concentrating solar plants. ACS Sustain Chem Eng. 2018; 6(5): 6404-17. https://doi.org/10.1021/acssuschemeng.8b00199

[5] Valverde JM, Barea-López M, Perejón A, Sánchez-Jiménez PE, Pérez-Maqueda LA. Effect of thermal pretreatment and nanosilica addition on limestone performance at calcium-looping conditions for thermochemical energy storage of concentrated solar power. Energy Fuels. 2017; 31(4): 4226-36. https://doi.org/10.1021/acs.energyfuels.6b03364

[6] Ho CK. A review of high-temperature particle receivers for concentrating solar power. Appl Therm Eng. 2016; 109(B): 958-69. https://doi.org/10.1016/j.applthermaleng.2016.04.103

[7] Kearney D, Kelly B, Herrmann U, *et al*. Engineering aspects of a molten salt heat transfer fluid in a trough solar field. Energy. 2004; 29(5-6): 861-70. https://doi.org/10.1016/S0360-5442(03)00191-9

[8] Vignarooban K, Xu X, Arvay A, Hsu K, Kannan AM. Heat transfer fluids for concentrating solar power systems—a review. Appl Energy. 2015; 146: 383-96. https://doi.org/10.1016/j.apenergy.2015.01.125

[9] Shah N, Arshad A, Khosa AA, Ali HM, Ali M. Thermal analysis of a mini solar pond of small surface area while extracting heat from lower convective layer. Therm Sci. 2019; 23(2A): 763-76.

[10] Cot-Gores J, Castell A, Cabeza LF. Thermochemical energy storage and conversion: a state-of-the-art review of the experimental research under practical conditions. Renew Sustain Energy Rev. 2012; 16(7): 5207-24. https://doi.org/10.1016/j.rser.2012.04.007

[11] Pardo P, Deydier A, Anxionnaz-Minvielle Z, Rougé S, Cabassud M, Cognet P. A review on high-temperature thermochemical heat energy storage. Renew Sustain Energy Rev. 2014; 32: 591-610. https://doi.org/10.1016/j.rser.2013.12.014

[12] Medrano M, Gil A, Martorell I, Potau X, Cabeza LF. State of the art on high-temperature thermal energy storage for power generation. Part 2—case studies. Renew Sustain Energy Rev. 2010; 14(1): 56-72. https://doi.org/10.1016/j.rser.2009.07.036

[13] Mohan G, Venkataraman MB, Coventry J. Sensible energy storage options for concentrating solar power plants operating above 600°C. Renew Sustain Energy Rev. 2019; 107: 319-37. https://doi.org/10.1016/j.rser.2019.01.062

[14] Nahhas T, Py X, Sadiki N. Experimental investigation of basalt rocks as storage material for high-temperature concentrated solar power plants. Renew Sustain Energy Rev. 2019; 110: 226-35. https://doi.org/10.1016/j.rser.2019.04.060

[15] Zalba B, Marín JM, Cabeza LF, Mehling H. Review on thermal energy storage with phase change: materials, heat transfer analysis and applications. Appl Therm Eng. 2003; 23(3): 251-83. https://doi.org/10.1016/S1359-4311(02)00192-8

[16] Nithyanandam K, Pitchumani R. Design of a latent thermal energy storage system with embedded heat pipes. Appl Energy. 2014; 126: 266-80. https://doi.org/10.1016/j.apenergy.2014.03.025

[17] Block T, Schmücker M. Metal oxides for thermochemical energy storage: a comparison of several metal oxide systems. Sol Energy. 2016; 126: 195-207. https://doi.org/10.1016/j.solener.2015.12.032

[18] Dizaji HB, Hosseini H. A review of material screening in pure and mixed-metal oxide thermochemical energy storage (TCES) systems for concentrated solar power (CSP) applications. Renew Sustain Energy Rev. 2018; 98: 9-26. https://doi.org/10.1016/j.rser.2018.09.004

[19] Chacartegui R, Alovisi A, Ortiz C, Valverde JM, Verda V, Becerra JA. Thermochemical energy storage of concentrated solar power by integration of the calcium looping process and a CO2 power cycle. Appl Energy. 2016; 173: 589-605. https://doi.org/10.1016/j.apenergy.2016.04.053

[20] Rhodes NR, Barde A, Randhir K, *et al*. Solar thermochemical energy storage through carbonation cycles of $SrCO_3$/SrO supported on $SrZrO_3$. ChemSusChem. 2015; 8(22): 3793-8. https://doi.org/10.1002/cssc.201501023

[21] Qu X, Li Y, Li P, Wan Q, Zhai F. The development of metal hydrides using as concentrating solar thermal storage materials. Front Mater Sci. 2015; 9: 317-31. https://doi.org/10.1007/s11706-015-0311-y

[22] Sattler C, Roeb M, Agrafiotis C, Thomey D. Solar hydrogen production via sulphur-based thermochemical water-splitting. Sol Energy. 2017; 156: 30-47. https://doi.org/10.1016/j.solener.2017.05.060

[23] Chen C, Aryafar H, Lovegrove KM, Lavine AS. Modeling of ammonia synthesis to produce supercritical steam for solar thermochemical energy storage. Sol Energy. 2017; 155: 363-71. https://doi.org/10.1016/j.solener.2017.06.049

[24] Hong H, Jin H, Ji J, Wang Z, Cai R. Solar thermal power cycle with integration of methanol decomposition and middle-temperature solar thermal energy. Sol Energy. 2005; 78(1): 49-58. https://doi.org/10.1016/j.solener.2004.06.019

[25] Schmidt M, Linder M. Power generation based on the $Ca(OH)_2$/CaO thermochemical storage system—experimental investigation of discharge operation modes in lab scale and corresponding conceptual process design. Appl Energy. 2017; 203: 594-607. https://doi.org/10.1016/j.apenergy.2017.06.063

[26] Romeo LM, Lara Y, Lisbona P, Martínez A. Economical assessment of competitive enhanced limestones for CO_2 capture cycles in power plants. Fuel Process Technol. 2009; 90(6): 803-11. https://doi.org/10.1016/j.fuproc.2009.03.014

[27] Cormos CC. Economic evaluations of coal-based combustion and gasification power plants with post-combustion CO_2 capture using calcium looping cycle. Energy. 2014; 78: 665-73. https://doi.org/10.1016/j.energy.2014.10.054

[28] N'Tsoukpoe KE, Liu H, Le Pierrès N, Luo L. A review on long-term sorption solar energy storage. Renew Sustain Energy Rev. 2009; 13(9): 2385-96. https://doi.org/10.1016/j.rser.2009.05.008

[29] Martínez A, Lara Y, Lisbona P, Romeo LM. Energy penalty reduction in the calcium looping cycle. Int J Greenh Gas Control. 2012; 7: 74-81. https://doi.org/10.1016/j.ijggc.2011.12.005

[30] Duelli G (Varela), Charitos A, Diego ME, Stavroulakis E, Dieter H, Scheffknecht G. Investigations at a 10 kWth calcium looping dual fluidized bed facility: limestone calcination and CO_2 capture under high CO_2 and water vapor atmosphere. Int J Greenh Gas Control. 2015; 33: 103-12. https://doi.org/10.1016/j.ijggc.2014.12.006

[31] Lee LM, Jang YN, Ryu KW, Kim W, Bang JH. Mineral carbonation of flue gas desulfurization gypsum for CO_2 sequestration. Energy. 2012; 47(1): 370-7. https://doi.org/10.1016/j.energy.2012.09.009

[32] N'Tsoukpoe KE, Restuccia G, Schmidt T, Py X. The size of sorbents in low-pressure sorption or thermochemical energy storage processes. Energy. 2014; 77: 983-98. https://doi.org/10.1016/j.energy.2014.10.013

[33] Perejón A, Miranda-Pizarro J, Pérez-Maqueda LA, Valverde JM. On the relevant role of solids residence time on their CO2 capture performance in the calcium looping technology. Energy. 2016; 113: 160-71. https://doi.org/10.1016/j.energy.2016.07.028

[34] Khosa AA, Yan J, Zhao CY. Investigating the effects of ZnO dopant on the thermodynamic and kinetic properties of $CaCO_3$/CaO TCES system. Energy. 2021; 215: 119132. https://doi.org/10.1016/j.energy.2020.119132

[35] Lu S, Wu S. Calcination-carbonation durability of nano CaCO3 doped with Li2SO4. Chem Eng J. 2016; 294: 22-9. https://doi.org/10.1016/j.cej.2016.02.100

[36] Khosa AA, Shah N, Han X, Naveed H. Silica dopant effect on the performance of calcium carbonate/calcium oxide-based thermal energy storage system. Therm Sci. 2024; 28(2A): 837-50. https://doi.org/10.2298/TSCI230422165K

[37] Jing JY, Li TY, Zhang XW, Wang SD, Feng J, Turmel WA, *et al*. Enhanced CO_2 sorption performance of $CaO/Ca_3Al_2O_6$ sorbents and its sintering-resistance mechanism. Appl Energy. 2017; 199: 225-33. https://doi.org/10.1016/j.apenergy.2017.03.131

[38] Jin D, Yu X, Yue L, Wang L. Decomposition kinetics study of AlOOH coated calcium carbonate. Mater Chem Phys. 2009; 115(1): 418-22. https://doi.org/10.1016/j.matchemphys.2008.12.013

[39] Wang Y, Zhu Y, Wu S. A new nano CaO-based CO_2 adsorbent prepared using an adsorption phase technique. Chem Eng J. 2013; 218: 39-45. https://doi.org/10.1016/j.cej.2012.11.095

[40] Chen H, Zhang P, Duan Y, Zhao C. Reactivity enhancement of calcium-based sorbents by doping with metal oxides through the sol-gel process. Appl Energy. 2016; 162: 390-400. https://doi.org/10.1016/j.apenergy.2015.10.035

[41] Yanase I, Maeda T, Kobayashi H. The effect of addition of a large amount of CeO_2 on the CO_2 adsorption properties of CaO powder. Chem Eng J. 2017; 327: 548-54. https://doi.org/10.1016/j.cej.2017.06.140

[42] Chen X, Jin X, Liu Z, Ling X, Wang Y. Experimental investigation on the CaO/CaCO3 thermochemical energy storage with SiO_2 doping. Energy. 2018; 155: 128-38. https://doi.org/10.1016/j.energy.2018.05.016

[43] Shui M, Yue L, Hua Y, Xu Z. The decomposition kinetics of the SiO_2 coated nano-scale calcium carbonate. Thermochim Acta. 2002; 386(1): 43-9. https://doi.org/10.1016/S0040-6031(01)00723-7

[44] Mathew A, Nadim N, Chandratilleke TT, Paskevicius M, Humphries TD, Buckley CE. Kinetic investigation and numerical modelling of $CaCO_3/Al_2O_3$ reactor for high-temperature thermal energy storage application. Sol Energy. 2022; 241: 262-74. https://doi.org/10.1016/j.solener.2022.06.005

[45] Coats AW, Redfern JP. Kinetic parameters from thermogravimetric data. Nature. 1964; 201(4914): 68-9. https://doi.org/10.1038/201068a0

[46] Achar BN, Brindley GW, Sharp JH. Kinetics and mechanism of dehydroxylation processes. III. Applications and limitations of dynamic methods. In: Proceedings of the International Clay Conference. Jerusalem: 1966.

[47] Kissinger HE. Reaction kinetics in differential thermal analysis. Anal Chem. 1957; 29(11): 1702-6. https://doi.org/10.1021/ac60131a045

[48] Khosa AA, Zhao C. Heat storage and release performance analysis of $CaCO_3$/CaO thermal energy storage system after doping nano silica. Sol Energy. 2019; 188: 619-30. https://doi.org/10.1016/j.solener.2019.06.048

[49] Xu TX, Tian XK, Khosa AA, Yan J, Ye Q, Zhao CY. Reaction performance of $CaCO_3$/CaO thermochemical energy storage with TiO_2 dopant and experimental study in a fixed-bed reactor. Energy. 2021; 236: 121451. https://doi.org/10.1016/j.energy.2021.121451

[50] Zhang M, He X, Xue Y, Lin Z, Tong NH, Lai W, Liang S. Improving thermoelectric properties of Cu2O powder via interface modification. Solid State Commun. 2022; 357: 114982. https://doi.org/10.1016/j.ssc.2022.114982

[51] Pan J, Liu G. Chapter Ten - Facet control of photocatalysts for water splitting. In: Mi Z, Wang L, Jagadish C, editors. Semiconductors and Semimetals. Elsevier; 2017, p. 349-91. https://doi.org/10.1016/bs.semsem.2017.04.003

[52] Vyazovkin S, Burnham AK, Criado JM, Pérez-Maqueda LA, Popescu C, Sbirrazzuoli N. ICTAC Kinetics Committee recommendations for performing kinetic computations on thermal analysis data. Thermochim Acta. 2011; 520(1): 1-19. https://doi.org/10.1016/j.tca.2011.03.034

[53] Webb PB, Dearnley JH, McConville JC. Characterization of metal oxide-carbonate composites by X-ray diffraction. J Appl Crystallogr. 2004; 37(5): 631-7.

[54] Sutherland BR, Williams AC, Blake CL. X-ray diffraction studies of calcium carbonate polymorphs. J Solid State Chem. 1980; 32(2): 148-54.

[55] Islam SM, Khan SMZS, Hasan MT. X-ray diffraction and optical studies of Cu_2O nanoparticles. Mater Chem Phys. 2014; 147(1-2): 238-44.

[56] Kim HS, Kim SM, Park SM. Optical properties of Cu_2O thin films and its application to optoelectronics. J Appl Phys. 2009; 106(12): 123512.

[57] Trinh TT, Chen CHK. Band gap and optical characteristics of $CaCO_3$. Mater Sci Eng B. 2015; 192: 37-42.

[58] Wang LW, Wang XY, Chen HX. Optical and electronic properties of metal oxide composites: Cu_2O and $CaCO_3$. J Compos Mater. 2015; 49(21): 2621-30.

[59] Akinmoladun AO, Ojo JO, Akinmoladun DT. FTIR and X-ray diffraction studies of Cu2O nanoparticles synthesized by chemical reduction method. J Nanomater. 2012.

[60] Reddy MM, Reddy VPV. Infrared and Raman spectroscopy of calcium carbonate and its polymorphs. J Mol Struct. 2000; 534(1-3): 1-16.